




# Fiber photometry for monitoring cerebral oxygen saturation in freely-moving rodents

LINHUI YU,<sup>1,2</sup>  ELIZABETH M. S. THURSTON,<sup>2,3,5</sup> MADA HASHEM,<sup>2,4,5</sup> JEFF F. DUNN,<sup>2,4</sup> PATRICK J. WHELAN,<sup>2,3</sup> AND KARTIKEYA MURARI<sup>1,2,\*</sup>

<sup>1</sup>University of Calgary, Schulich School of Engineering, Electrical and Computer Engineering, Calgary, Canada

<sup>2</sup>University of Calgary, Hotchkiss Brain Institute, Calgary, Canada

<sup>3</sup>University of Calgary, Department of Neuroscience, Calgary, Canada

<sup>4</sup>University of Calgary, Biomedical Engineering Graduate Program, Calgary, Canada

<sup>5</sup>These authors contributed equally to this work

\*[kmurari@ucalgary.ca](mailto:kmurari@ucalgary.ca)

**Abstract:** Hemodynamic parameters, such as tissue oxygen saturation and blood volume fraction, are important markers of brain physiology. They are also widely used surrogate markers of electrophysiological activity. Here, we present a single fiber spectroscopic (SFS) system for monitoring cerebral oxygen saturation in localized, non-line-of-sight brain regions in freely-moving rodents. We adapted the implantation ferrule and patch cable design from commercialized optogenetics and fiber photometry systems, enabling stereotaxic fiber implantation, longitudinal tissue access and measurement from freely-moving animals. The optical system delivers and collects light from the brain through a 200  $\mu\text{m}$ -core-diameter, 0.39NA multimode fiber. We robustly measured oxygen saturation from phantoms with different optical properties mimicking brain tissue. In mice, we demonstrated, for the first time, measurements of oxygen saturation from a highly-localized, targeted brain region over 31 days and continuous measurements from a freely-moving animal for over an hour. These results suggest that single fiber spectroscopy has enormous potential for functional brain monitoring and investigating neurovascular coupling in freely-moving animals. In addition, this technique can potentially be combined with fiber photometry systems to correct for hemodynamic artifacts in the fluorescence detection.

© 2020 Optical Society of America under the terms of the [OSA Open Access Publishing Agreement](#)

## 1. Introduction

Brain activity consumes oxygen, which is carried by hemoglobin in red blood cells. Therefore, brain activity leads to vascular responses, and the resulting changes in blood-related-parameters can be used as surrogates for investigating brain function. Hemoglobin is an intrinsic light absorber, with distinct absorption features in the visible and near-infrared wavelengths that vary depending on whether or not it is oxygen-bound [1]. For this reason, intrinsic optical signals, *e.g.* scattering and absorption, are widely applied for measuring hemodynamic parameters, such as vessel diameter, blood flow, oxygen saturation ( $\text{sO}_2$ ) and blood volume fraction, as a surrogate measure of neuronal activity. Hemodynamic parameters are most commonly studied using functional magnetic resonance imaging (fMRI), functional near infrared spectroscopy (fNIRS) and intrinsic optical imaging. Measuring hemodynamic parameters is essential to understanding neurovascular coupling, the relationship between neuronal activity and vascular responses. It is also critical for properly interpreting the blood-oxygen-level-dependent (BOLD) signals commonly used in fMRI of the human brain [2].

Moreover, since intrinsic optical contrasts are inherent in tissue, any changes in the hemodynamic parameters also affect the performance of optical stimulation and optical measurements

using extrinsic optical contrasts [3]. Thus, accurate measurement of intrinsic optical signals is needed for high-fidelity optical measurements and stimulation in tissue.

Hemodynamic parameters can only be studied *in-vivo*, and a majority of experiments are conducted in animal models. Due to scattering and absorption, optical techniques have limited depth penetration in brain tissue. Systems using near-infrared wavelengths, e.g. NIRS, can reach deep brain structures but at the cost of sampling a large volume, while systems using visible wavelengths can sample from a small, but superficial, volume of tissue [1]. Moreover, conventional optical systems usually require animals to be anesthetized or restrained. Specialized systems that enable functional brain monitoring from freely-moving animals provide measurements of brain activity in close-to-natural conditions [4]. There has been an increasing interest in conducting imaging studies in freely-moving animals. However, it is very challenging to design miniaturized systems within the size, weight, power constraints while retaining performance [5].

Single fiber optical systems provide a practical approach to achieve minimal invasiveness and a small sample volume in deep brain structures. The fiber probe can be stereotactically implanted into the region of interest at any depth to measure from a small volume of tissue near the fiber tip. Currently, single fiber optical systems are most commonly used for techniques based on extrinsic optical contrasts, e.g. fiber photometry for measuring  $\text{Ca}^{2+}$  signals [6,7], fluorophore-coated probes for partial pressure of oxygen ( $\text{pO}_2$ ) [8] and temperature [9] measurements. Fiber photometry systems are often used to measure from freely-moving animals.

Single fiber optical systems have also been used to measure intrinsic optical signals. Examples include optical biopsying to detect cancerous tissue and diagnostic devices for diseases like hepatic steatosis and intervertebral disc mineralization. Some of these systems provide quantitative measures such as chromophore concentrations [10,11], scatterer sizes [12], scattering intensity [13,14] or the refractive index [15]. However, the focus is on a binary discrimination between tissue states. Compared to such applications, challenges for functional hemodynamic monitoring include the small magnitude and transient nature of the changes.

Previously, we have presented a single fiber spectroscopic system for measuring oxygen saturation in non-line-of-sight regions in the brain in anesthetized animals [16]. The volume of tissue probed by the system was estimated to be 0.02-0.03 mm<sup>3</sup> from Monte Carlo simulations. We demonstrated *in-vivo* measurement in anesthetized mice with controlled inhaled oxygen level, and the stimulus-evoked oxygen saturation response from anesthetized rats under deep brain stimulation [17]. However, the system was sensitive to fiber movement due to fiber birefringence, and could not be used with freely-moving animals. This was because we used linear polarizers to minimize back-reflections at the air-fiber interface.

In this paper, we present an improved system design of the single fiber spectroscopic system for measuring intrinsic optical signals in the brain, utilizing an angle-polished fiber to reject back-reflections. We designed an implantation ferrule based on standard optogenetic stimulation and fiber photometry systems. Therefore, existing experimental protocols can be adapted, enabling stereotaxic targeting, longitudinal measurements and applications in freely-moving animals. We focus on reporting the instrumentation design, system calibration and validation in pilot longitudinal experiments from freely-moving animals.

## 2. Methods

### 2.1. System design

Figure 1 shows a schematic drawing of the optical system, adapted from the design of optogenetic stimulation and fiber photometry systems. A neutral white light-emitting-diode (LED, XQ-E High Intensity, Cree) powered with a constant current source is used as the light source. A 300  $\mu\text{m}$  diameter pinhole (#56-285, Edmund Optics) is put in touch with the LED to limit the image size and therefore reduce the reflection from the fiber near end.

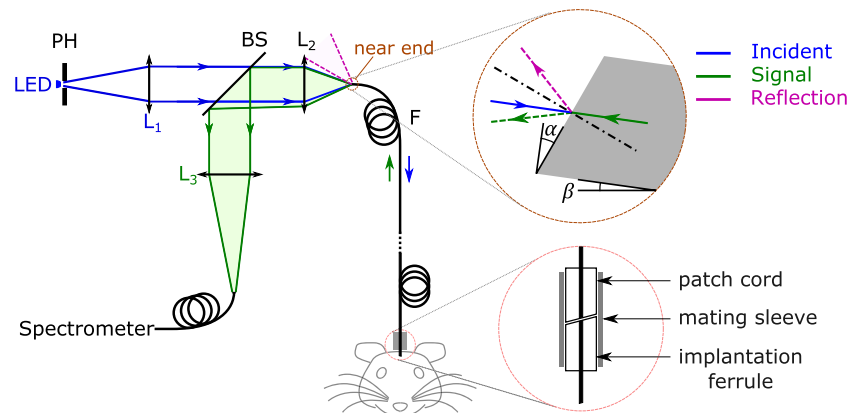


**Fig. 1.** Schematic drawing of the single fiber system design utilizing angle-polishing to reduce Fresnel reflection. In the delivery path (blue), light from an LED is collimated by a lens ( $L_1$ ). 50 % of light passes the 50:50 beam splitter (BS), and is focused by lens  $L_2$  into a fiber patch cord (F) with both ends terminated in steel ferrules polished at  $16^\circ$ . A pinhole (PH) is used to limit the image size. An implantation ferrule, or optrode, with both ends polished at  $16^\circ$  is implanted into the target brain region in an animal. During measurements, the patch cord is connected to the implantation ferrule using a ceramic mating sleeve. In the collection path (green), signal light coming out of the fiber is collimated by  $L_2$ . At the beam splitter (BS), 50 % of the signal light is reflected  $90^\circ$ .  $L_3$  focuses this light into a fiber connected to a spectrometer. A magnified view of the fiber near end shows the directions of the incident and signal light. The normal to the fiber face makes an angle  $\alpha$  with the optical axis, and the fiber is tilted at an angle  $\beta$ . Therefore, the angle between the air-fiber interface and the optical axis is  $(\alpha + \beta)$ . The reflected incidence (magenta) and the refracted signal (green) go in opposite directions.

In the delivery path (marked in blue) of the benchtop system, light from the LED is collimated by a lens ( $L_1$ , AC127-019-A, Thorlabs). A 50:50 beam splitter (BS) transmits 50 % of the light which is focused into the near end of a ferrule-terminated, 200- $\mu\text{m}$ -core, 0.39 NA fiber patch cord (F, FT200UMT, Thorlabs) by a second lens ( $L_2$ , A240-A, Thorlabs). The remaining 50 % light is reflected towards an absorbing beam dump to avoid stray reflections. The fiber guides the light to and collects light from the target volume of tissue.

To reduce the amount of reflection from the fiber interfaces reaching the detector, all fiber surfaces are angle polished to reduce Fresnel reflections. At the near end of the patch cord, the reflected incidence (magenta) and the refracted signal (green) go towards opposite directions. Based on Zemax simulations, when the near end is polished at  $24^\circ$ , the Fresnel reflections from the fiber near end will not be detected. Instead of polishing the fiber at  $24^\circ$ , an angle-polish and tilt approach was used. We avoid using a larger polishing angle for the following reasons: i) polishing a fiber at a larger angle requires the removal of larger amount of material, both from the fiber ferrule and the fiber itself; ii) at larger polishing angles, the fiber end face has a greater surface area and it is more difficult to achieve a high-quality polish; iii) the signal light deviates more from the optical axis with larger polishing angle, and therefore, reduces the collection efficiency of the signal light. For the final design, the near end of the patch cord is polished at  $16^\circ$  and is tilted at  $8^\circ$  along the optical axis, with the final angle being  $24^\circ$ .

We customized a stainless steel ferrule (SF230-10, Thorlabs) to hold a piece of multimode fiber using heat-curable epoxy (353NDPK, Thorlabs) for implantation into the target brain region. Both ends were polished at  $16^\circ$ . This implantation ferrule is compatible with standard stereotaxic frames with cannula holders [18]. The far end of the fiber patch cable is terminated with the same

stainless steel ferrule and polished at 16° to mate with the implantation ferrule. A mating sleeve (ADAF1, Thorlabs) is used to connect the far end of patch cord and the implantation ferrule.

Light exits the fiber at the far end, enters and interacts with the brain region of interest, undergoing scattering and absorption. Some of this light, which constitutes the signal, enters the same optical fiber, and travels back to the near end. In the collection path (marked in green), the light coming out of the fiber is collimated by L<sub>2</sub>. Then, half of this light is reflected 90°, and focused into a spectrometer (Maya2000Pro, Ocean Optics) by a focusing lens (L<sub>3</sub>, AC127-019-A, Thorlabs). We limited experiment durations to under a few hours and did not use a rotary joint.

## 2.2. System calibration

Previously, we reported a calibration method using the reflections from the fiber-sample interface to approximate the spectrum of the light entering tissue [16]. We revised the calibration process considering that the angle-polished fiber far end minimizes the reflections from the fiber-sample interface. The reflectance spectrum  $R_{SF}$  can be calculated as

$$R_{SF} = \frac{S_{sam} - S_{gly}}{(S_{air} - S_{gly}) \cdot r} \quad (1)$$

where  $S$  is the spectrum, subscripts *sam*, *gly* and *air* denote measurement in the sample, glycerin and air, respectively and  $r$  is a correction factor depending on fiber dispersion. The spectrum measured in glycerin accounts for residual reflections from the fiber near end. The numerator ( $S_{sam} - S_{gly}$ ) measures the signal light with the attenuation in the collection path. The denominator ( $S_{air} - S_{gly}$ ) is a measure of the Fresnel reflection from the fiber far end when it is in the air. It estimates the spectrum of the light exiting the fiber with the attenuation in the collection path. However, due to dispersion in the fiber, the light which exits the fiber and these reflections have different spectra. To account for this difference, we introduced the correction factor  $r$  which is the ratio of transmission to reflection at different wavelengths considering dispersion of the fiber used. This was estimated with simulations using the fiber parameters.

$$r(\lambda) = \frac{T(\lambda)}{R(\lambda)} \quad (2)$$

where  $T$  and  $R$  are the transmission and reflection at the fiber far end when it is in the air.

To operate the single fiber spectroscopic system, the LED and the spectrometer were turned on at least 30 minutes before the measurement started to allow them to warm up. Next, two reference spectra were measured; first, when the fiber far end was in the air ( $S_{air}$ ) and then when it was immersed in glycerin ( $S_{gly}$ ). The fiber was then put in touch with the sample and the spectra recording started. In post-processing, the reflectance spectra ( $R_{SF}$ ) were calculated using Eq. (1). Oxygen saturation values were then estimated by fitting the data to the model described above using lsqcurvefit, an implementation of a nonlinear least-squares solver, in MATLAB [16].

## 2.3. Characterization in tissue phantom

The single fiber spectroscopic system was characterized in tissue phantom experiments. Similar to the experiments described previously [16], the liquid phantom contains intralipid as the scatterer and rat blood as the absorber. Previously, we utilized a commercial device (OxyLite, Oxford Optronix) for measuring partial pressure of oxygen as the reference. To convert pO<sub>2</sub> to oxygen saturation using the oxygen dissociation curve, accurate measurements of the pH, carbon dioxide partial pressure and 2,3-diphosphoglyceric acid concentration in the phantom are required. This is challenging, and others have concluded that it is not practical to convert pO<sub>2</sub> to oxygen saturation accurately [19]. NIRS measures oxygen saturation based on intrinsic optical signals in the near infrared band. However, a comparison of commercially available, and laboratory-built

NIRS systems showed significant variation [19,20] and there is no universally accepted reference standard. Thus, we chose to simultaneously monitor the phantom with a custom built broadband NIRS system [21], not to quantify performance but to have some redundancy in the measurement.

The NIRS system we used measured the attenuation spectrum across 705-960 nm at a rate of 2 Hz through separate source and detection fibers with a 20 mm separation. Data processing involved multilinear regression to fit the second derivative of the measured attenuation spectra to the specific extinction coefficients of deoxygenated hemoglobin leading to an estimate of its concentration [22]. To measure oxygen saturation, the total hemoglobin concentration  $C_{Hbt}$  is required. In the phantom, we assume that all the hemoglobin was deoxygenated at the end of the experiment when the phantom was in a pure nitrogen environment for a long time, *i.e.*  $C_{Hbt} = C_{Hb}$ . Oxygen saturation can then be calculated as:

$$sO_2\% = \frac{C_{Hbt} - C_{Hb}}{C_{Hbt}} \times 100\% \quad (3)$$

Fig. 2 shows a schematic drawing of the phantom experiment set up. The liquid phantom was kept in an airtight box. A stir bar was used to keep the phantom homogeneous. The NIRS system and the single fiber spectroscopic system measured from the phantom simultaneously. Care was taken to place the fibers of the two systems such that no cross-talk could be detected.

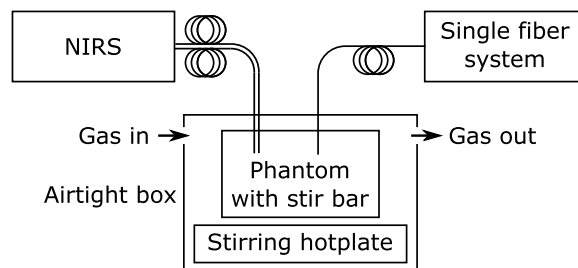


**Fig. 2.** A schematic of the experimental setup for system validation in a phantom.

First, 1.2 mL rat blood was added into the liquid phantom containing 60 mL of 1 % intralipid and phosphate buffered saline leading to a 2 % blood volume fraction. The airtight box was infused with pure oxygen until the blood was assumed to be fully oxygenated. Then, measurements began, and the pure oxygen was replaced with pure nitrogen to deoxygenate the phantom. When oxygen saturation was assumed to have reached 0 %, another 0.6 mL of rat blood was added, making the blood volume fraction ~3 %. Pure oxygen was used to oxygenate the blood again. Then, a second recording session started, and nitrogen was introduced into the box again.

#### 2.4. Animal preparation

We adapted an optogenetic stimulation protocol for animal preparation [23]. Two 9-week old male C57BL/6 mice (Charles River Laboratories, Senneville) were implanted with the custom ferrules just above the A11 region in the posterior hypothalamus. The mice were anesthetized by inhaled isoflurane (4 % for induction, 1.5-2 % for maintenance, mixed with pure oxygen at 0.5 L/min). Then, the animal was placed onto a stereotaxic frame and the head was secured. The scalp was exposed and a small burr hole was made with a sterile drill bit (skull coordinates: AP 2.30 mm, ML 0.10 mm). The ferrule was placed in a holder, which allowed precise implantation to target the brain structure, and the ferrule was lowered into the brain (DV -3.0 mm). The implantation ferrule was secured with Metabond (K-Dental Inc.) and Dentsply (Dentsply International Inc.). After the cement was cured, the scalp around the implantation ferrule was sutured. Animals were given buprenorphine and lidocaine for analgesia. One set of measurements was taken while



the animals were still under anesthesia. The animals were then returned to the home cage for recovery, and monitored for 48 hours post-surgery. All animal experiments were conducted in accordance with Canadian Council for Animal Care guidelines, and were approved by the Health Sciences Animal Care Committee of the University of Calgary.

### 2.5. Longitudinal measurements

To test whether the system could measure oxygen saturation robustly from animals, measurements were taken on days 2, 3, 4, 7, 14, 21, and 31 after the implantation. The animal was induced under 4 % isoflurane mixed with pure oxygen. The exposed faces of the implantation ferrule and the fiber patch cable was cleaned with ethanol and delicate task wipes. Then, the fiber patch cable was connected to the implantation ferrule using a ceramic ferrule sleeve. Glycerin was used as the matching medium to fill the air gap between the interfaces of the two fiber ferrules to minimize coupling losses. Spectra were recorded continuously while the animal was under the maintenance of anesthesia (0.25-1 % isoflurane) for ~5 minutes. Then the isoflurane and oxygen were removed, and the animals breathed room air. Measurements continued at least until the animals recovered and started to move freely, walking and grooming. Durations ranged from 3 to 30 minutes after removing anesthesia. After the measurements were done, the fiber patch cable was disconnected, and the animal was returned to its home cage.

When the animal breathes in isoflurane mixed with pure oxygen, we expect to see higher oxygen saturation in the brain than when the animal breathes room air (21 % oxygen). Thus, as the animal recovers from anesthesia under room air, the oxygen saturation level should drop.

### 2.6. Measurements with controlled inhaled oxygen

The previous experiment had a single change in oxygen level as the animal recovers. While the animal was freely moving, there were no further systemic changes. To cause controlled changes in oxygen saturation while the animal is freely moving, we used a sealed chamber measuring 12"× 9"×9" with a controlled oxygen supply. The experiment was conducted on day 21 after implantation. The implantation ferrule was connected to the system as described above. Next, the animal was put in the air chamber, and the spectroscopic measurements started. Oxygen and nitrogen mixture with different oxygen percentage was delivered into the box. An OxyLite (OxyLite Pro, Oxford Optronix) was used to measure the  $pO_2$  in the box. The  $pO_2$  probe was mounted near the top of the box such that the animal would not be able to reach it, but we assumed the gas content in the box was homogeneous.

## 3. Results

### 3.1. System design

Figure 3(A) shows a photograph of the implantation ferrule. The red arrows point out the surface of the angle-polished ferrule and the fiber tip. Figure 3(B) shows a zoomed-in view of the angle-polished fiber tip. Figure 3(C) shows a photograph of a mouse implanted with the customized fiber ferrule and the connection from the animal to the benchtop system with the customized patch cord and mating sleeve.

### 3.2. Characterization in tissue phantom

Figure 4 shows the measured reflectance spectra and the fitted spectra at different oxygen saturation values in the tissue phantoms with 2 % and 3 % blood volume fraction (BVF). The fitted spectra captured most of the features in the measured spectra. The magnitude of the reflectance spectra measured in the 3 % blood volume phantom were lower than the spectra measured in the 2 % blood volume fraction phantom, indicating there was more blood and therefore stronger absorption in the phantom.

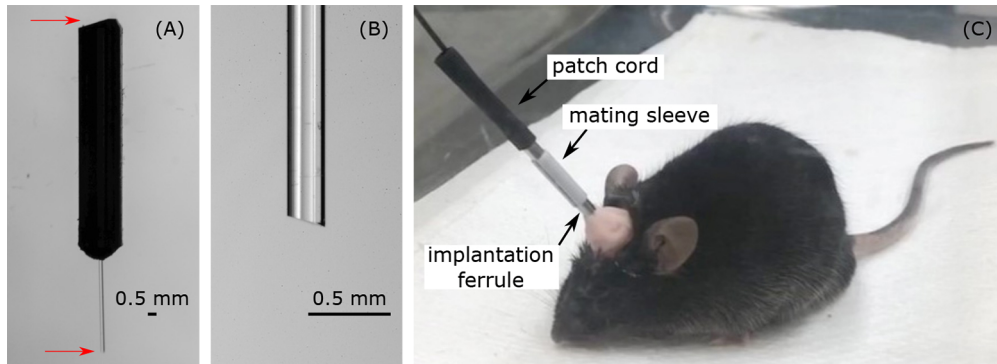


**Fig. 3.** (A) Photograph of the implantation ferrule. The arrows point out the polished ferrules and fiber tip. (B) Zoomed-in view of the polished fiber tip. (C) A photograph showing a mouse implanted with the customized ferrule and the connection from the animal to the benchtop system with a patch cord and a mating sleeve.

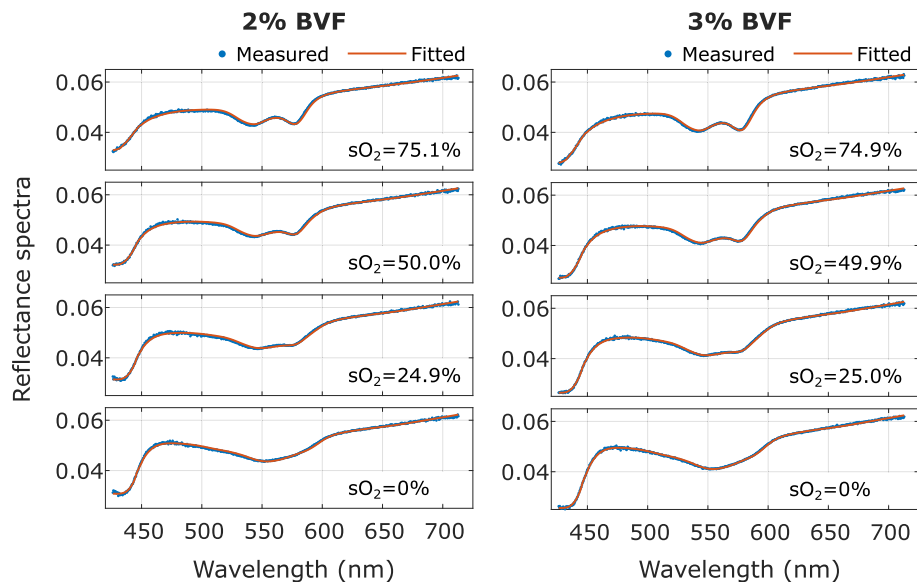


**Fig. 4.** Reflectance spectra and fitted spectra from the optical phantom with 2 % and 3 % blood volume fraction. Oxygen saturation values were measured by the single fiber spectroscopic system.

Figure 5 shows the oxygen saturation values measured by the SFS and NIRS in the two phantom tests. In the 3 % optical phantom, the measurement started when the oxygen saturation was approximately 70 % estimated by the NIRS system. Across both blood fractions, the root mean square and maximum differences between SFS and NIRS were 5.9 % and 12 %.

Due to the lack of an exact reference, we can not judge accuracy. However, both systems responded monotonically to changes in oxygen saturation. SFS, and to a lesser extent NIRS, estimated negative values at very low oxygen saturations, while NIRS seemed to saturate at very high oxygen saturations.

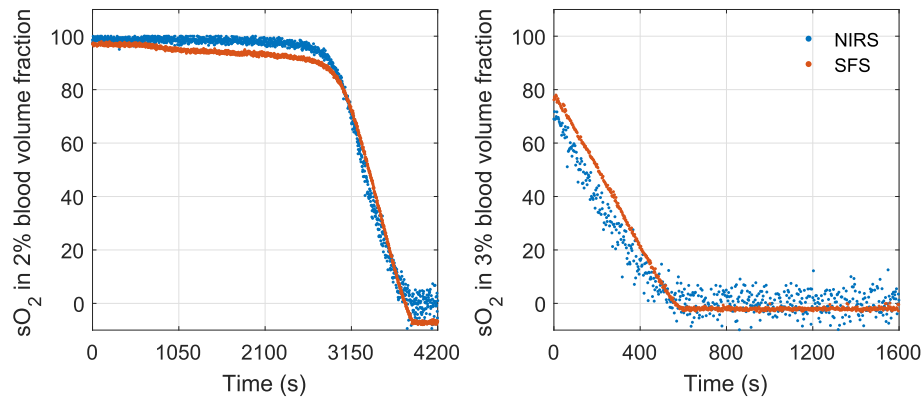


**Fig. 5.** Oxygen saturation estimated by NIRS and SFS in an optical phantom at two blood fractions. Root mean square difference was 5.9 %, and both systems were monotonic across the entire range.

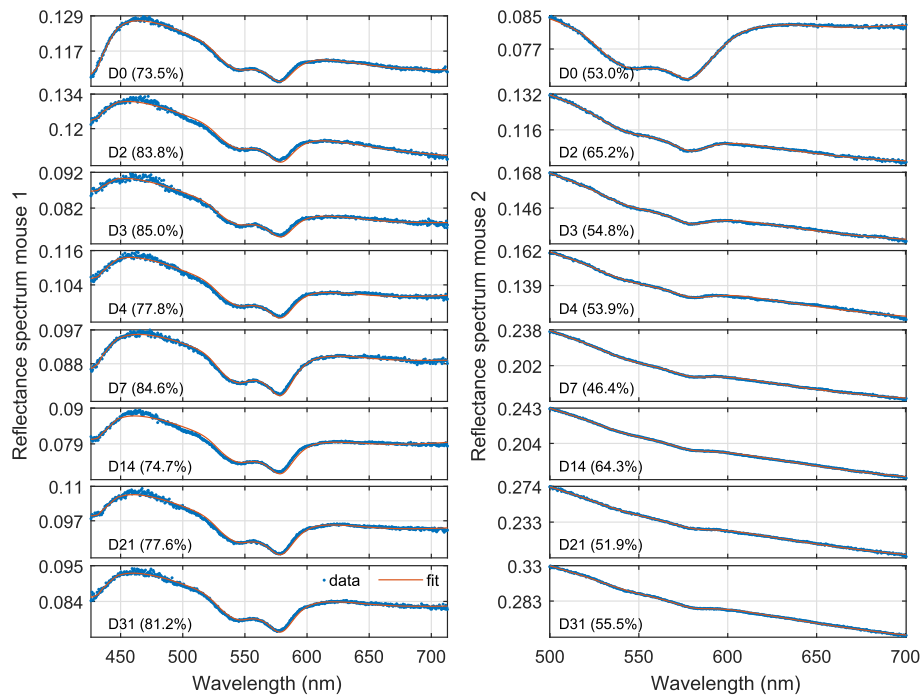
### 3.3. Longitudinal experiments

Figure 6 shows the reflectance spectra, the fitted spectra, and the extracted oxygen saturation, while Mouse 1 and Mouse 2 were under isoflurane mixed with pure oxygen. Oxy-hemoglobin has two absorption peaks in the 500-700 nm range. Two reflectance valleys can be seen in all the spectra, indicating that the hemoglobin is mostly oxygenated. For Mouse 1, the magnitude of the reflectance spectra remained steady and shifted slightly from day to day, which may be due to the variability in the coupling efficiency on different days of the experiments. The integration time used for the measurements was 12 ms on Day 0, and 15 ms on all other days. Five consecutive spectra were averaged leading to a measurement rate of 13.3-16.7 Hz. The oxygen saturation extracted from the spectra varies from 74-84 %. In Mouse 2, amplitudes of the reflectance spectra were higher than those in Mouse 1, indicating higher scattering and lower absorption. The integration time used for the measurement decreased from 15 ms on Day 0 to 8 ms on Day 31, as the intensity of reflectance spectra increased over time. Since the fitting process to extract oxygen saturation relies on absorptive features in the spectrum, lower absorption implies lower signal quality. To compensate for this, 10 or 20 consecutive spectra were averaged, leading to a lower overall sampling frequency between 6.3-13.3 Hz. Only the spectral features in 500-700 nm were used for fitting. The oxygen saturation extracted ranged from 46-65 %.

Pigment packaging tends to reduce the observed absorption as hemoglobin is restricted within vessels [24]. On the Day 0, relatively less light in the blue wavelengths (~430 nm) was measured than the measurements on all other days, indicating the absorption in that region was strongest on Day 0. This suggests that the effect of pigment packaging was minimal on Day 0. This could be due to local bleeding during the fiber implantation surgery leading to extravascular blood surrounding the tip of the fiber.

Figure 7(A) shows the oxygen saturation trends as Mouse 1 and Mouse 2 recovered from anesthesia measured across Day 2 to Day 31. During the first 45 s, the animals were under isoflurane mixed with pure oxygen. Then, the animals were switched to breathing room air. Data is shown for a subsequent 180 s, by when the animals were grooming and walking. Note that these time series were manually aligned, because the time of taking the animal off isoflurane and pure oxygen was recorded at minute resolution in most of the experiments. The baseline oxygen saturation varied across days, but stayed steady while the animals were under isoflurane. When the isoflurane and pure oxygen was turned off and the animals breathed in room air, a drop in the oxygen saturation was observed in every measurement. There was minimal variation in the





**Fig. 6.** Reflectance spectra, fitted spectra and extracted oxygen saturation measured from the brain of Mouse 1 and Mouse 2 under isoflurane mixed with pure oxygen on different days. Five spectra were averaged for Mouse 1. For Mouse 2, 10 spectra were averaged on Days 2-4 and 20 spectra were averaged on subsequent days.

oxygen saturation while the animals were under anesthesia. However, towards the end of the experiments, as the animals were awake and freely moving, there were small variations in oxygen saturation, which could be indicators of local brain activity.

Figure 7(B) shows the relative changes in oxygen saturation from 5 seconds before, to 25 seconds after, the switch from isoflurane with pure oxygen to room air measured across Day 2 to Day 31 from Mouse 1 and Mouse 2. Reductions of ~10 % and ~5-10 % in oxygen saturation happened in ~10 seconds after switching the inhalation in Mouse 1 and Mouse 2, respectively.

On Day 31, there were large variations starting at ~80 s in Mouse 1. An analysis of the data (Fig. 11 in [Appendix](#)) showed small changes in the reflectance spectra consistent with small changes in oxygen saturation. This suggests the oxygen saturation variations extracted from the spectra may not be artifacts.

Figure 8 shows representative examples of longer duration oxygen saturation measurements from both mice. While Fig. 7 highlights the transition from anesthetized to freely-moving conditions, these data further demonstrate measurements from freely-moving animals. The oxygen saturation dropped for about 400-500 s after switching the inhaled oxygen level, then stabilized with small variations that may be indicative of brain activity.

### 3.4. Measurements with controlled inhaled oxygen

Figure 9 shows the  $sO_2$  values measured from Mouse 1 on Day 21 over a period of an hour as it was freely-moving in the controlled air chamber. The blue dashed lines mark the changes in the oxygen levels in the air chamber. In the course of the experiment, the animal breathed in pure oxygen prior to being put in the box, and the oxygen percentages that were infused into the box

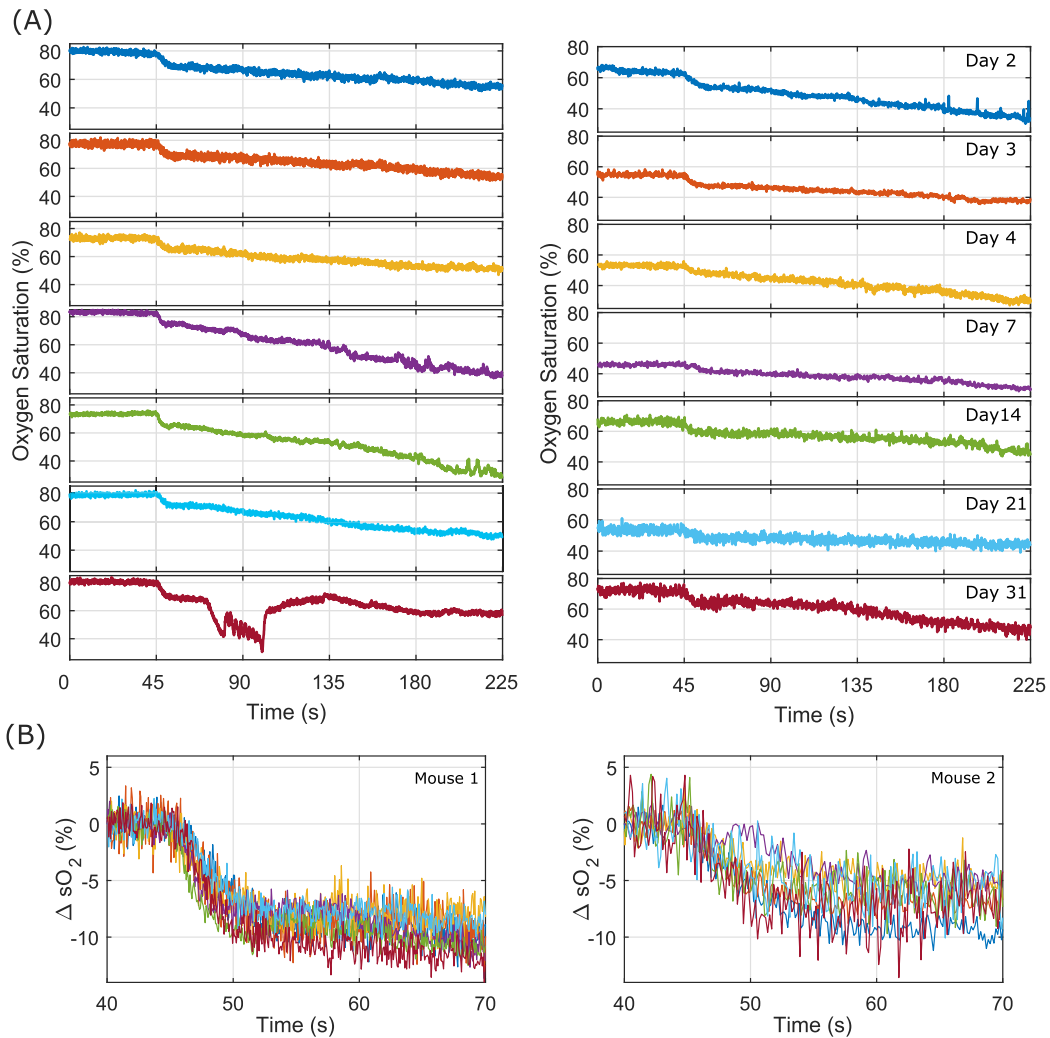


**Fig. 7.** (A) Oxygen saturation in Mouse 1 (left) and Mouse 2 (right) as they recovered from anesthesia, measured across Day 2 to Day 31. For 0-45 s, the animals breathed isoflurane mixed with pure oxygen. From 45-225 s, the animals breathed room air. (B) Relative changes in oxygen saturation measured from Mouse 1 (left) and Mouse 2 (right) when the inhaled air changed from isoflurane and pure oxygen to room air.

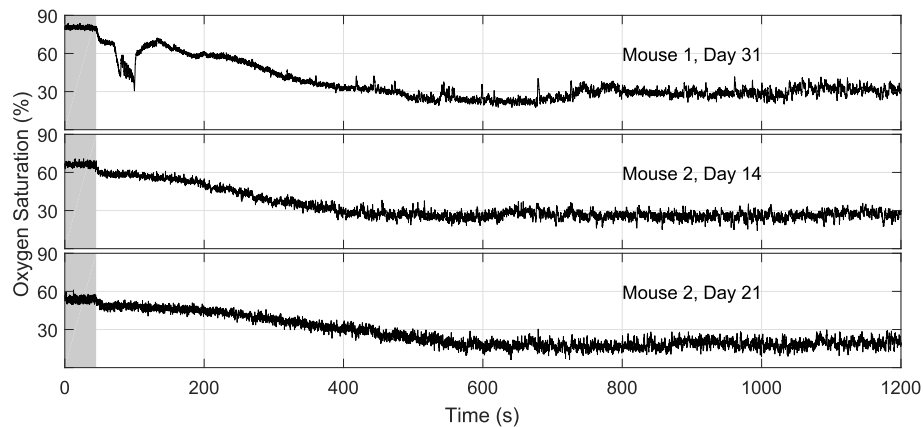


**Fig. 8.** Oxygen saturation measured from Mouse 1 on Day 31 and from Mouse 2 on Day 14 and 21. The shaded region indicated the time when the animals were breathing isoflurane mixed with pure oxygen. After the first few minutes, the animals were fully awake and moved freely in their home cages with the lids open.

were 21 %, 8 %, 15 % and finally 30 %. The gray line shows the raw  $sO_2$  measurement, while the black trace shows the  $sO_2$  measurement filtered by a median filter with a width of 30 samples ( $\sim 2$  s). The red trace shows the  $pO_2$  values measured by the OxyLite. The OxyLite readings had a delay of approximately 60 s compared to the time when the oxygen level was changed. This delay cannot be corrected because the OxyLite has a specified response time of less than 20 s [25], rather than a constant latency, and its data acquisition system time delay was also not clear. The duration of time for the oxygen to diffuse to the  $pO_2$  sensor was also not quantified.

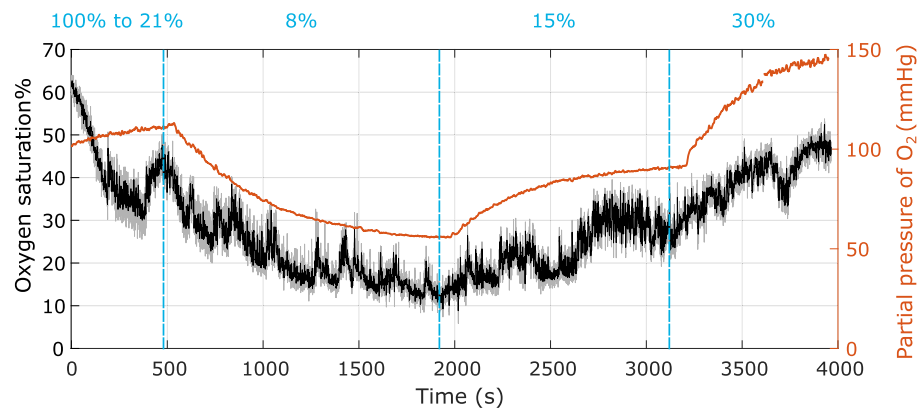


**Fig. 9.** Oxygen saturation measured with the SFS from a freely-moving mouse in an airtight box with controlled oxygen level. Gray trace shows the extracted oxygen saturation, black trace shows oxygen saturation filtered by a median filter with a width of 30 samples ( $\sim 2$  s). The red trace shows the  $pO_2$  in the box measured with the OxyLite probe. The experiment started with 21 % of oxygen in the box, however, the mouse was under pure oxygen and isoflurane before being put into the box, thus for the animal the inhaled oxygen level changed from pure oxygen to 21 %. Then, the oxygen level in the box was switched to 8 %, 15 % and 30 % at indicated times.

At first,  $sO_2$  went down from  $\sim 60$  %, because the animal was under isoflurane and pure oxygen, and then the inhaled oxygen level dropped to 21 % when the animal was put in the chamber. The

general trend of  $sO_2$  looks similar to the  $pO_2$  trend. However, there were small variations of the  $sO_2$ , which may be caused by local brain activity causing changes in the hemodynamics.

### 3.5. Histology

The brains of the mice were harvested and sliced after 13 weeks from implantation. Figure 10 shows micrographs of brain slices from both animals stained with cresyl violet. The fiber track can be clearly observed. The tissue near the fiber tip looks similar to tissue away from the implant track, indicating no significant photodamage or trauma was induced by the delivery of light through the fiber implant.

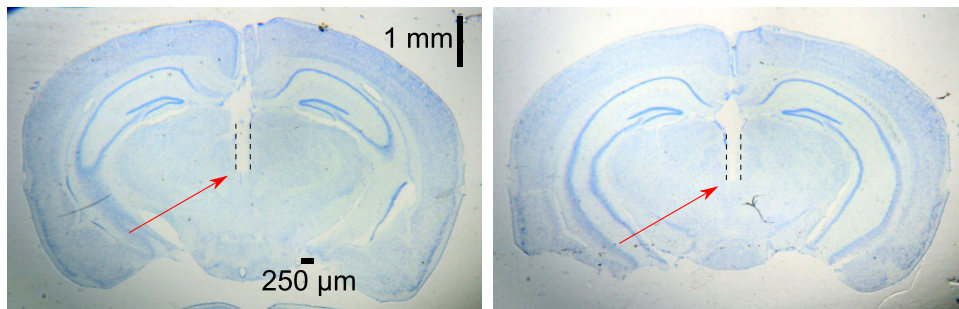


**Fig. 10.** Micrographs of brain slices showing the fiber implant tracks in both mice. The red arrow points to the end of the track.

## 4. Discussion

### 4.1. System design

We use an angle-polished fiber to separate the reflected incidence and the signal light. Thus, the new system is less sensitive to fiber movement compared to the previous system which suffers the extra sensitivity induced by fiber birefringence. This greatly increases the utility of this technique since it allows for experiments in freely-moving animals. A simpler calibration process is proposed for calculating reflectance spectrum. We adapted the fiber patch cable and implantation ferrule used in optogenetic stimulation and fiber photometry systems and successfully utilized an optogenetic stimulation surgical protocol for longitudinal measurements in freely moving animals.

The sampling rates when measured in freely-moving animals were over  $\sim 15$  Hz. The system is fast enough for measuring hemodynamic response, which usually happens on the time scale of seconds [4]. The LED was powered by 0.5 A constant current, therefore, the sampling rate can be further increased if needed. The optical power going into the tissue was approximately  $130 \mu\text{W}$  over a  $200 \mu\text{m}$  diameter area, and is below the safety threshold [26].

### 4.2. Characterization in tissue phantom

In the experiments with tissue phantoms, various phantom conditions provided the first comprehensive assessment of the performance of the single fiber spectroscopic system in measuring relative changes. We controlled the partial pressure of oxygen in the environment to induce changes in oxygen saturation. For our airtight box of volume 20 L and about 60 mL phantom, it could take more than 1 hour for the oxygen saturation in the phantom to change from approximately 100 % to 0 %. Both SFS and NIRS estimated monotonic changes in the correct direction and had a root mean square difference of 5.9 %. Both systems showed negative oxygen saturation values at low oxygen saturations. NIRS only measures deoxyhemoglobin concentration and requires an

estimate of the total hemoglobin concentration. An underestimate can lead to negative oxygen saturation values from Eq. (3). In SFS, inaccuracies in the absorption coefficients, as well as the linear assumption of reflectance caused by scattering alone, may cause the fitting to return negative numbers [16]. There is no universally accepted gold standard technique to calibrate the measurement of oxygen saturation accurately, even in a controlled phantom setting. Kleiser et al. reported a variation of over 40 % in oxygen saturation among several commercial and lab-built systems [19,20]. Thus, the aim of our tissue phantom experiments was not to quantify the absolute accuracy of the system, but to guide the interpretation of *in vivo* data. Nevertheless, these experiments support the conclusion that the single fiber spectroscopic system robustly measures changes in oxygen saturation.

#### 4.3. Longitudinal experiments

We experimentally demonstrated longitudinal oxygen saturation measurements in deep brain regions through implantation ferrules across 31 days in freely-moving animals. As for oxygen saturation extracted from the measured spectra, in both animals across Day 2 to Day 31, similar trends were observed when the inhaled air changed from isoflurane and pure oxygen to room air. Though the magnitude of the measured reflectance spectra changed across days, the oxygen saturation estimation depends on absorption features that govern the shape of the spectrum. Thus we were able to measure oxygen saturation in anesthetized animals with a standard deviation of 4.2 and 5.9 % in two mice in 8 measurement sessions across 31 days. These measurements demonstrated that SFS was able to measure reflectance spectra and extract oxygen saturation values from a highly-localized volume robustly over a month.

#### 4.4. Measurements with controlled inhaled oxygen

The general trend of oxygen saturation and the partial pressure of oxygen in the air chamber matched with each other. There were unexplained small fluctuations in oxygen saturation, probably indicating local functional activation or movement artifact, as they were not observed in the data when mice were under anesthesia as shown in Fig. 7. The fiber was implanted in A11, a brain region whose function is currently unclear, but has been recently shown to evoke locomotor activity when stimulated [23,27].

Histological examination of cresyl violet stained brain slices indicated tissue had recovered from the trauma caused by the fiber implantation procedure. No visible damage was seen due to the excitation light. The light power delivered into the brain was on the order of 100  $\mu$ W, which is well below the tissue damage threshold. The sampling rate of the system can be further improved by increasing the driving current of the light source.

#### 4.5. Future work

One potential application is to combine the proposed single fiber spectroscopic system with a fiber photometry system. This may enable i) concurrent measurement of neuronal activity using calcium indicators or voltage-sensitive dyes, and the related hemodynamic response; ii) accurate measurements using extrinsic optical contrast, overcoming the bias of hemodynamic artifacts.

Using the proposed system, we may be able to measure the hemodynamic response from the same volume of tissue as the optogenetic stimulation, and potentially from freely-moving animals. Such a system may enable all-optical closed-loop optogenetic stimulation.

### 5. Conclusions

We presented a single fiber spectroscopic system for measuring oxygen saturation through a small diameter fiber from the brain of freely-moving animals. It consists of a benchtop spectroscopic system that can be connected to a ferrule implanted at a brain region of interest



with a fiber patch cord and a mating sleeve. The system is compatible with standard optogenetic stimulation and fiber photometry techniques. To the best of our knowledge, this study was the first demonstration of monitoring oxygen saturation longitudinally from a highly-localized deep brain region in a freely-moving animal. Tissue phantom experiments showed that the system responded monotonically to changes in oxygen saturation. As the absolute accuracy was not measured, oxygen saturation values need to be interpreted with care. The sampling rate in *in-vivo* experiments was between 6-15 Hz, and it can be further increased if needed. The optical power used was on the order of 100  $\mu$ W. No visible photodamage was observed on brain slices. Previous Monte Carlo (MC) simulations have estimated the measurement tissue volume between 0.02-0.03 mm<sup>3</sup> [16].

Recently, multimodal systems have been reported for correcting the hemodynamic artifact, *i.e.* a distortion of fluorescence signals due to changes in the blood perfusion and oxygen saturation. This has been applied to spectral imaging systems measuring from the brain surface [3,28], but fiber photometry systems still suffer from hemodynamic artifacts [29]. We believe our intrinsic-signal-based single fiber system has the potential to enable multimodal measurements and correct for hemodynamic artifacts in the fluorescence channel.

Taken together, these results suggest that single fiber spectroscopy has enormous potential for investigating neurovascular coupling in freely-moving animals.

## Appendix

On Day 31, there were large variations starting at ~80 seconds. Figure 11(A) shows a zoomed-in view of these variations. Figure 11(B-C) show four spectra measured at the times of the peaks and the valleys of the variations, marked by the '+' markers in (A). Changes in shape, especially at lower than 450 nm and at 525-600 nm, can be seen in the reflectance spectra. This suggests the oxygen saturation variations extracted from the spectra may not be artifacts.

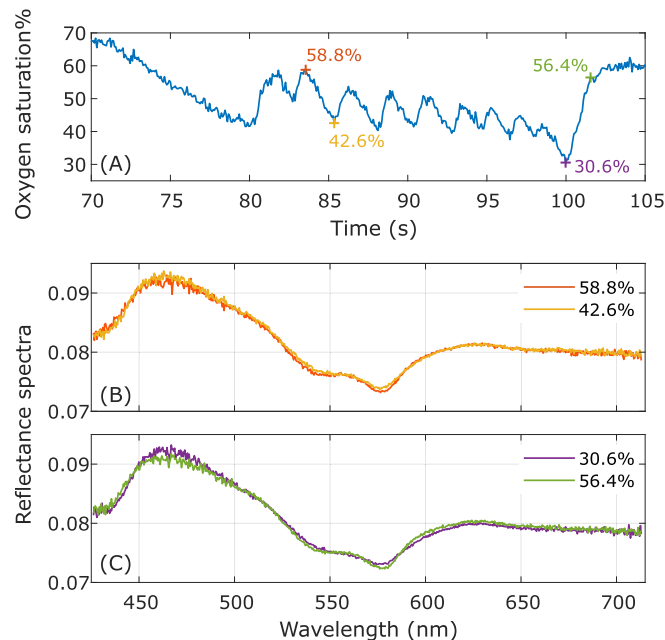


**Fig. 11.** (A) Zoomed in view of the oxygen saturation variations measured on Day 31 from Mouse 1. (B) and (C) show the reflectance spectra at the times marked by the colored marks in (A).

## Funding

Natural Sciences and Engineering Research Council of Canada; Hotchkiss Brain Institute, University of Calgary; University of Calgary.

## Acknowledgments

We would like to thank Dr. Ying Wu and Nicole Orsi Barioni for assistance in experimental preparation and histology, respectively. We also thank Dr. Zelma Kiss, Dr. Elise Fear and Linda Kim for helpful discussions. This research was supported by University of Calgary, Hotchkiss Brain Institute, and the Natural Sciences and Engineering Research Council.

## Disclosures

The authors declare no conflicts of interest.

## References

1. T. Vo-Dinh, *Biomedical Photonics Handbook, 3 Volume Set* (CRC Press, 2014).
2. E. M. Hillman, "Optical brain imaging in vivo: techniques and applications from animal to man," *J. Biomed. Opt.* **12**(5), 051402 (2007).
3. Y. Ma, M. A. Shaik, S. H. Kim, M. G. Kozberg, D. N. Thibodeaux, H. T. Zhao, H. Yu, and E. M. Hillman, "Wide-field optical mapping of neural activity and brain haemodynamics: considerations and novel approaches," *Philos. Trans. R. Soc., B* **371**(1705), 20150360 (2016).
4. Y.-R. Gao, Y. Ma, Q. Zhang, A. T. Winder, Z. Liang, L. Antinori, P. J. Drew, and N. Zhang, "Time to wake up: Studying neurovascular coupling and brain-wide circuit function in the un-anesthetized animal," *NeuroImage* **153**, 382–398 (2017).
5. H. Yu, J. Senarathna, B. M. Tyler, N. V. Thakor, and A. P. Pathak, "Miniaturized optical neuroimaging in unrestrained animals," *NeuroImage* **113**, 397–406 (2015).
6. L. A. Gunaydin, L. Grose, J. C. Finkelstein, I. V. Kauvar, L. E. Fenno, A. Adhikari, S. Lammel, J. J. Mirzabekov, R. D. Airan, K. A. Zalocusky, K. M. Tye, P. Anikeeva, R. C. Malenka, and K. Deisseroth, "Natural neural projection dynamics underlying social behavior," *Cell* **157**(7), 1535–1551 (2014).
7. T. N. Lerner, C. Shilyansky, T. J. Davidson, K. E. Evans, K. T. Beier, K. A. Zalocusky, A. K. Crow, R. C. Malenka, L. Luo, R. Tomer, and K. Deisseroth, "Intact-brain analyses reveal distinct information carried by SNc dopamine subcircuits," *Cell* **162**(3), 635–647 (2015).
8. K. Lee, S. Bohnert, Y. Wu, C. Vair, J. Mikler, G. C. Teskey, and J. F. Dunn, "Assessment of brain oxygenation imbalance following soman exposure in rats," *NeuroToxicology* **65**, 28–37 (2018).
9. S. T. Musolino, E. P. Schartner, M. R. Hutchinson, and A. Salem, "Improved method for optical fiber temperature probe implantation in brains of free-moving rats," *J. Neurosci. Methods* **313**, 24–28 (2019).
10. S. C. Kanick, C. Van der Leest, J. G. Aerts, H. C. Hoogsteden, S. Kaščáková, H. J. Sterenborg, and A. Amelink, "Integration of single-fiber reflectance spectroscopy into ultrasound-guided endoscopic lung cancer staging of mediastinal lymph nodes," *J. Biomed. Opt.* **15**(1), 017004 (2010).
11. S. H. Tabrizi, F. Farzaneh, S. M. R. Aghamiri, M. Arab, M. Hosseini, T. Ashrafganjoei, and M. Chehrizi, "Comparison between performance of single-fiber reflectance spectroscopy (SFRS) system and colposcopy: a phase III trial," *Lasers Med. Sci.* **32**(9), 2139–2144 (2017).
12. T. Denkçeken, T. Şimşek, G. Erdoğan, E. Peştereli, Ş. Karaveli, D. Özel, U. Bilge, and M. Canpolat, "Elastic light single-scattering spectroscopy for the detection of cervical precancerous ex vivo," *IEEE Trans. Biomed. Eng.* **60**(1), 123–127 (2013).
13. D. Piao, K. L. McKeirnan, N. Sultana, M. A. Breshears, A. Zhang, and K. E. Bartels, "Percutaneous single-fiber reflectance spectroscopy of canine intervertebral disc: Is there a potential for in situ probing of mineral degeneration?" *Lasers Surg. Med.* **46**(6), 508–519 (2014).
14. D. Piao, J. W. Ritchey, G. R. Holyoak, C. R. Wall, N. Sultana, J. K. Murray, and K. E. Bartels, "In vivo percutaneous reflectance spectroscopy of fatty liver development in rats suggests that the elevation of the scattering power is an early indicator of hepatic steatosis," *J. Innovative Opt. Health Sci.* **11**(04), 1850019 (2018).
15. X. U. Zhang, D. J. Faber, A. L. Post, T. G. van Leeuwen, and H. J. Sterenborg, "Refractive index measurement using single fiber reflectance spectroscopy," *J. Biophotonics* **12**(7), e201900019 (2019).
16. L. Yu, Y. Wu, J. F. Dunn, and K. Murari, "In-vivo monitoring of tissue oxygen saturation in deep brain structures using a single fiber optical system," *Biomed. Opt. Express* **7**(11), 4685–4694 (2016).
17. L. Yu, M. S. Noor, Z. H. Kiss, and K. Murari, "Hemodynamic monitoring in different cortical layers with a single fiber optical system," in *Neural Imaging and Sensing 2018*, vol. 10481 (International Society for Optics and Photonics, 2018), p. 104811H.

18. "Stereotaxic cannula holders," <http://doriclenses.com/life-sciences/cannulas-stereotaxic-tools/823-stereotaxic-cannula-holders.html>. Accessed: 2020-05-12.
19. S. Kleiser, N. Nasser, B. Andresen, G. Greisen, and M. Wolf, "Comparison of tissue oximeters on a liquid phantom with adjustable optical properties," *Biomed. Opt. Express* **7**(8), 2973–2992 (2016).
20. S. Kleiser, D. Ostojic, B. Andresen, N. Nasser, H. Isler, F. Scholkmann, T. Karen, G. Greisen, and M. Wolf, "Comparison of tissue oximeters on a liquid phantom with adjustable optical properties: an extension," *Biomed. Opt. Express* **9**(1), 86–101 (2018).
21. Q. Zhang, S. Srinivasan, Y. Wu, S. Natah, and J. F. Dunn, "A near-infrared calibration method suitable for quantification of broadband data in humans," *J. Neurosci. Methods* **188**(2), 181–186 (2010).
22. M. Hashem, Q. Zhang, Y. Wu, T. W. Johnson, and J. F. Dunn, "Using a multimodal near-infrared spectroscopy and mri to quantify gray matter metabolic rate for oxygen: A hypothermia validation study," *NeuroImage* **206**, 116315 (2020).
23. K. Koblinger, C. Jean-Xavier, S. Sharma, T. Fuzesi, L. Young, S. Eaton, C. H. Kwok, J. Bains, and P. J. Whelan, "Optogenetic activation of A11 region increases motor activity," *Front. Neural Circuits* **12**, 86 (2018).
24. R. Van Veen, W. Verkrusse, and H. Sterenberg, "Diffuse-reflectance spectroscopy from 500 to 1060 nm by correction for inhomogeneously distributed absorbers," *Opt. Lett.* **27**(4), 246–248 (2002).
25. "Oxford optronix: Oxygen monitors," <https://www.oxford-optronix.com/en/Oxygen-Monitors>. Accessed: 2019-11-21.
26. S. F. Owen, M. H. Liu, and A. C. Kreitzer, "Thermal constraints on in vivo optogenetic manipulations," *Nat. Neurosci.* **22**(7), 1061–1065 (2019).
27. K. Koblinger, T. Füzési, J. Ejdrygiewicz, A. Krajacic, J. S. Bains, and P. J. Whelan, "Characterization of A11 neurons projecting to the spinal cord of mice," *PLoS One* **9**(10), e109636 (2014).
28. B. B. Scott, S. Y. Thiberge, C. Guo, D. G. R. Tervo, C. D. Brody, A. Y. Karpova, and D. W. Tank, "Imaging cortical dynamics in gcamp transgenic rats with a head-mounted widefield macroscope," *Neuron* **100**(5), 1045–1058.e5 (2018).
29. A. Devor, S. Sakadžić, M. A. Yaseen, E. Roussakis, P. Tian, H. Slovin, I. Vanzetta, I. Teng, P. A. Saisan, L. E. Sinks, A. M. Dale, S. A. Vinogradov, and D. A. Boas, "Functional imaging of cerebral oxygenation with intrinsic optical contrast and phosphorescent probes," in *Optical Imaging of Neocortical Dynamics*, (Springer, 2014), pp. 225–253.